Neuropeptide feedback modifies odor-evoked dynamics in *C. elegans* olfactory neurons

Sreekanth H. Chalasani[1], **Saul Kato**[1,2], **Dirk R. Albrecht**[1], **Takao Nakagawa**[1], **L. F. Abbott**[2], and **Cornelia I. Bargmann**[1,3]

[1]Howard Hughes Medical Institute, The Rockefeller University, NY, New York 10065

[2]Department of Neuroscience, Department of Physiology and Cellular Biophysics, Columbia University College of Physicians and Surgeons, New York, NY 10032-2695

Abstract

Many neurons release classical transmitters together with neuropeptide cotransmitters whose functions are incompletely understood. Here we define the relationship between two transmitters in the olfactory system of *Caenorhabditis elegans*, showing that a neuropeptide-to-neuropeptide feedback loop alters sensory dynamics in primary olfactory neurons. The AWC olfactory neuron is glutamatergic and also expresses the peptide NLP-1. *nlp-1* mutants have increased AWC-dependent behaviors, suggesting that NLP-1 limits the normal response. The receptor for NLP-1 is the G protein-coupled receptor NPR-11, which acts in postsynaptic AIA interneurons. Feedback from AIA interneurons modulates odor-evoked calcium dynamics in AWC olfactory neurons and requires INS-1, a neuropeptide released from AIA. The neuropeptide feedback loop dampens behavioral responses to odors on short and long timescales. Our results point to neuronal dynamics as a site of behavioral regulation and reveal the ability of neuropeptide feedback to remodel sensory networks on multiple timescales.

Embedded in an animal's neuroanatomy are the pathways that drive its behavior. Over twenty years ago, a wiring diagram of the *C. elegans* nervous system was constructed from serial-section electron micrographs1. Despite this unique resource, the relationships between sensory inputs, neuronal activity, and specific behavioral programs are unclear2, 3. We are exploring these issues within a circuit that generates undirected search when animals are removed from food, and directed chemotaxis in odor gradients4–6. Both of these behaviors are initiated by AWC olfactory neurons and are based upon temporally-regulated turning: when animals are removed from food, a transient bout of turning produces undirected local search, and in the presence of an odor gradient, temporally-regulated turning produces a biased random walk for gradient climbing7, 8. Through cell ablation and quantitative behavioral analysis, neurons in this circuit have been traced from sensory input to motor

[3]Author for correspondence; cori@rockefeller.edu.

output5, 6. Sensory neurons detect changes in odor levels or feeding state, and synapse onto a layer of interneurons that control turning rates in a coordinated fashion; a second layer of interneurons and downstream motor neurons regulate specific classes of turns and features of turns. The turning circuit has interesting temporal properties. First, even in a constant odor environment, an intrinsic process generates apparently stochastic turns. Second, to move up a spatial odor gradient using a biased random walk, animals calculate the time derivative of the odor signal over seconds. Third, odor history and food regulate the overall turning rate on a longer timescale of minutes. A meaningful understanding of this circuit must include neuronal properties that represent these varied behavioral timescales.

The neuropeptide gene *nlp-1* limits local search behavior

Previous studies demonstrated that AWC releases the neurotransmitter glutamate, which activates AIB interneurons via the glutamate-gated cation channel GLR-1 and inhibits AIY interneurons via the glutamate-gated chloride channel GLC-39 (Fig. 1a). AWC also expresses genes that encode predicted neuropeptides, including the buccalin-related peptide NLP-110. We characterized the function of NLP-1 by examining local search behavior, in which animals increase their turning rates during the initial 15 minutes after they are removed from food. Local search depends on AWC activity, and the rate of turning provides a quantitative measurement of AWC signaling6. A null mutant for *nlp-1*, generously provided by the *C. elegans* knockout consortium, had a higher turning rate than wild-type animals during local search (Fig. 1b). Like wild-type animals, *nlp-1* mutants suppressed turning after 15 minutes off food (Supplementary Table 1). This behavioral profile suggests that *nlp-1* inhibits AWC-induced turning behavior.

NLP-1 reporter genes are expressed in AWC, ASI, PHB, and BDU neurons and in the intestine10. The enhanced turning defect in *nlp-1* mutants was rescued by transgenic expression of *nlp-1* in AWC neurons, but not by expression in ASI neurons (Fig. 1b, Supplementary Table 1). Overexpression of *nlp-1* in AWC neurons of wild-type animals reduced the turning rate during local search (Fig. 1b). The opposite effects of *nlp-1* null mutants and gain-of-function transgenes suggest that this neuropeptide can be an instructive determinant of turning rates.

AWC-dependent turning behavior is reduced in mutants in the vesicular glutamate transporter gene *eat-4* or in the glutamate receptors *glr-1* or *glc-3*, defects opposite to those of *nlp-1* mutants9. Double mutants between *nlp-1* and *eat-4, glr-1*, or *glc-3* had reduced turning rates, resembling the mutants that affected glutamate signaling (Fig. 1b). This result suggests that NLP-1 functions as a cotransmitter whose effects are only apparent when the classical transmitter glutamate is also released: glutamate from AWC stimulates turning, and NLP-1 from AWC decreases the magnitude of this effect.

NLP-1 acts through the G protein-coupled receptor NPR-11

The *C. elegans* genome encodes about 100 G protein-coupled receptors (GPCRs) related to characterized neuropeptide receptors (www.wormbase.org). To identify the receptor for NLP-1, we examined GPCRs that lack known ligands, focusing on those for which expression has been observed in neurons connected to AWC11, 12. The orphan GPCR

NPR-11, whose closest characterized homolog is the *Drosophila* neuropeptide F receptor 1, was one candidate. We found that *npr-11* null mutants, like *nlp-1* mutants, had increased turning during AWC-dependent local search behavior (Fig. 1c, Supplementary Table 1).

nlp-1 npr-11 double mutants resembled the single mutants in turning behavior, the expected result for a ligand-receptor pair that acts together and not additively (Fig. 1c). In addition, the *npr-11* mutation fully suppressed the effects of *nlp-1* overexpression on turning behavior (Fig. 1c). This result indicates that *npr-11* is necessary for the biological activity of *nlp-1*, as predicted if *npr-11* encodes an *nlp-1* receptor.

npr-11 reporter genes are expressed in two postsynaptic targets of AWC, the AIA and AIY interneurons, and in other neurons[11] (data not shown). The *npr-11* behavioral defect in local search behavior resembled the defect after AIA interneurons are killed with a laser[9], and the *npr-11* defect was fully rescued by transgenic *npr-11* expression in AIA interneurons under the *gcy-28.d* promoter (Fig. 1c). These results suggest that NLP-1 release from AWC activates the NPR-11 GPCR on AIA. In agreement with this hypothesis, the turning behavior of *nlp-1 npr-11* double mutants was rescued only when *nlp-1* was expressed in AWC and *npr-11* was expressed in AIA together in the same strain (Fig. 1c, Supplementary Table 1).

A biochemical confirmation of the genetically inferred ligand-receptor relationship for NLP-1 and NPR-11 was obtained by expressing NPR-11 in HEK 293 cells together with the promiscuous G-protein α16Z13, and exposing the cells to synthesized peptide corresponding to one of four predicted MSFamide peptides encoded by *nlp-1*, MDANAFRMSFamide. NPR-11-expressing cells responded to micromolar concentrations of the peptide with calcium transients typical for GPCR activation (Fig. 1d). No responses were observed in response to scrambled NLP-1 peptide, in untransfected cells, or in cells expressing receptor or G-protein alone (Fig. 1d,e).

AWC inhibits AIA interneurons through glutamate and NLP-1 neurotransmitters

The relationship between AWC and AIA interneurons was examined directly using genetically-encoded calcium indicators of the G-CaMP family, which increase their fluorescence emission upon calcium binding[14,15]. *C. elegans* neurons are thought to lack sodium-based action potentials, but express voltage-gated calcium channels[16], and calcium signals in these neurons correlate with neuronal depolarization[17–22]. Previous experiments suggest that AWC neurons have basal activity at rest, are hyperpolarized by odor addition, and are strongly activated by odor removal[9]. We found that AIA interneurons had an opposite response, showing large transient calcium increases upon odor addition (Fig. 2a,b). Odor responses in AIA required AWC sensory input, as they were strongly attenuated when AWC neurons were killed using a laser microbeam (Fig. 2c,d). These results suggest that AWC forms inhibitory synapses onto AIA, as previously suggested for the synapses between AWC and AIY (Fig. 1a)[9]. In the simplest model, basal AWC activity at rest tonically inhibits AIA; when odor is added, AWC is hyperpolarized, tonic inhibition of AIA is reduced, and AIA becomes active.

Both glutamate and NLP-1 neurotransmitters contributed to odor-evoked calcium responses in AIA. AIA responses to odor were diminished in *eat-4* mutants that lack the vesicular glutamate transporter, and in *glc-3* mutants that lack a glutamate-gated chloride channel (Fig. 2e,f). The involvement of *glc-3* is consistent with its known expression in AIA, its molecular identity as an inhibitory glutamate-gated channel, and the prediction that the AWC-to-AIA synapse is inhibitory[11, 23]. *nlp-1* mutants also had a diminished response in AIA interneurons, which was partly rescued by expression of *nlp-1* in AWC neurons (Fig. 2g). The partial rescue of *nlp-1* may be due to variable expression of transgenes or to a combined action of *nlp-1* in AWC and additional neurons.

Although a dual action of glutamate and NLP-1 on AIA calcium signals was consistent with the behavioral analysis, the relationship between the transmitters was unexpected. In turning behavior, glutamate and NLP-1 had opposite effects, but in AIA calcium imaging experiments, the effects of *nlp-1* and *glc-3* were congruent. This distinction suggests that the behavioral effect of NLP-1 cannot be entirely explained by its observed effect on AIA activity, and prompted further examination of neurons in the AWC circuit.

AWC responses are modulated by NLP-1

The activity of sensory neurons such as AWC is thought to be defined primarily by sensory input, and not by network interactions. Unexpectedly, calcium imaging of the odor-evoked response in AWC neurons revealed alterations in *nlp-1* mutants. In both wild-type and *nlp-1* animals, initial calcium responses to odor removal peaked within ten seconds of odor removal (Fig. 3a–c, Supplementary Figs. S1, S2). However, in *nlp-1* mutants, the first peak was frequently followed by large secondary calcium transients that continued for at least two minutes after odor removal, the longest duration that was practical for calcium imaging (Fig. 3b,c). Thus NLP-1 neuropeptide signaling suppressed AWC calcium transients at long times after odor removal.

To provide a quantitative description of the altered activity in *nlp-1* mutants, a discrete Fourier transform was used to analyze the temporal character of the AWC calcium response to odor removal. Fourier analysis is well suited to reveal oscillatory or repeating signals, which appeared by inspection to be present in *nlp-1* traces. Indeed, spectral analysis suggested the existence of increased power in a mid-frequency domain in *nlp-1* mutants, with a significantly greater contribution than wild type from periodic components between 0.033 Hz - 1 Hz (period 1 – 30s) (Fig. 3d). The effects were statistically detectable at all time points, and suggest the presence of irregular slow oscillations with a preferred period near 20s. Cell-selective transgenic expression of *nlp-1* in AWC resulted in partial but significant rescue of the defect (Fig. 3c,d, Supplementary Fig. S1). The irregular oscillating signal was not observed in the absence of odor, excluding trivial optical or mechanical artifacts (Supplementary Fig. S1), but it was observed to some degree in wild-type traces as well as *nlp-1* traces, suggesting that it is a component of the normal AWC response.

Enhanced secondary AWC calcium signals were also observed in *npr-11* mutants after odor removal (Fig. 3e–g Supplementary Figs. S1,S2). Normal AWC calcium signals were restored by transgenic expression of *npr-11* in AIA neurons (Fig. 3g,h, Supplementary Fig.

S1). The functional effect of a receptor in AIA on odor responses in AWC strongly suggests the existence of feedback from AIA to AWC. In summary, these results suggest that NLP-1 release from AWC, sensed by NPR-11 in AIA, results in feedback onto AWC that suppresses secondary calcium transients after odor removal.

If modulatory feedback from the circuit contributes to normal AWC activity, other synaptic mutants could also affect AWC odor responses. Indeed, AWC responses to odor removal were reduced in *eat-4* mutants, which lack glutamatergic transmission from AWC and other neurons, and prolonged in *unc-31* mutants, which have reduced neuropeptide release from all neurons (Supplementary Fig. S2c,d)24, 25. These results suggest that the long-lasting AWC responses to odor removal are affected by synaptic inputs, with positive inputs from glutamatergic neurons and negative inputs from peptidergic neurons.

nlp-1 mutants are defective in AWC odor adaptation

The results described above suggest effects of neuropeptide signaling and feedback on long-lasting dynamics in AWC neurons. The 15 minute local search behavior is one sustained AWC-dependent behavior; a second sustained AWC-dependent behavior is olfactory adaptation, a behavioral change in which prolonged exposure to an odor leads to reduced chemotaxis to that odor (Fig. 4a,b)26. *nlp-1* and *npr-11* mutants failed to adapt to odors after a 60 min exposure (Fig. 4b), although they did adapt after a 90 minute exposure (Supplementary Fig. S3a). Like the defects in local search behavior, the olfactory adaptation defects were rescued by transgenic expression of *nlp-1* in AWC and transgenic expression of *npr-11* in AIA, respectively (Fig. 4b).

Previous studies have identified signaling components required cell-autonomously for olfactory adaptation in AWC, including GPCR regulators, TRPV channels, and a cGMP-dependent protein kinase27–32. However, the effects of adaptation on AWC activity have not been described. We found that wild-type animals adapted to odor for 60 minutes failed to respond to odor removal with AWC calcium transients, suggesting that adaptation blocked an early step of AWC signaling (Fig. 4c). By contrast, both *nlp-1* and *npr-11* mutants that had been exposed to odor for 60 minutes responded with AWC calcium transients after odor removal (Fig. 4c,d). Transgenic expression of *nlp-1* in AWC and *npr-11* in AIA neurons restored the wild-type AWC calcium response (Fig. 4c,d). These results indicate that NLP-1 release from AWC, acting on the NPR-11 receptor in AIA, generates feedback that reduces the primary AWC response to odor removal after adaptation.

INS-1 is a candidate feedback signal from AIA

The results described above suggest that AIA releases a signal that suppresses odor-evoked calcium responses in AWC. The insulin-related neuropeptide INS-1, which is expressed in AIA, modulates the function of the ASE gustatory neurons in a salt conditioning assay33, suggesting INS-1 as a possible signal from AIA to sensory neurons. Therefore, *ins-1* mutants were examined for their effects on AWC-regulated behaviors. Like *nlp-1* and *npr-11* mutants, *ins-1* mutants had increased turning in AWC-dependent local search behavior (Fig. 5a, Supplementary Table 1). Double mutants between *ins-1* and *nlp-1* resembled each single mutant, suggesting that these genes act in a common process (Fig.

5a). An *ins-1* mutation fully suppressed the effects of NLP-1 overexpression on turning behavior, suggesting that *ins-1* activity is necessary for the biological effects of *nlp-1* (Fig. 5a).

ins-1 is expressed in multiple neurons including AIA, RIC, ASI, and AWC33. Transgenic expression of *ins-1* from an AIA-selective promoter rescued turning behavior in the *ins-1* mutant, but expression from AWC, ASI, or RIC promoters did not (Fig. 5a, Supplementary Table 1, and data not shown). These results suggest a specific requirement for *ins-1* in AIA neurons. In double mutant studies, *nlp-1 ins-1* double mutants were restored to normal turning behavior only when *nlp-1* was expressed in AWC and *ins-1* was also expressed in AIA (Fig. 5a). *nlp-1(overexpressor) ins-1* double mutants were restored to the behavior of *nlp-1(overexpressor)* strains when *ins-1* was expressed in AIA (Fig. 5a). These experiments support a site of *ins-1* action in AIA neurons.

In calcium imaging experiments, *ins-1* mutants had secondary AWC transients after odor removal, with temporal properties similar to *nlp-1* and *npr-11* mutants (Fig. 5b, Supplementary Fig. S4). AIA specific expression of *ins-1* significantly rescued the altered odor response in AWC neurons, suggesting that AIA neuropeptides influence AWC activity (Fig. 5b, Supplementary Fig. S4).

ins-1 was also required for AWC-dependent olfactory adaptation. Like *nlp-1* and *npr-11* mutants, *ins-1* mutants did not adapt after a 60 min exposure to odor, but did adapt partially after 90 minutes (Fig. 5c, Supplementary Fig. S3). Adaptation in *nlp-1 ins-1* double mutants was similar to adaptation in each single mutant, suggesting that these two genes affect a common pathway (Supplementary Fig. S3c). Moreover, AWC neurons in *ins-1* animals exposed to odors for 60 minutes showed a calcium response after odor removal, unlike wild-type animals in the same conditions (Fig. 5d). Both the behavioral adaptation and the neuronal correlate of adaptation observed in calcium imaging were rescued by transgenic expression of *ins-1* in AIA (Fig. 5c,d Supplementary Fig. S3). These results suggest that INS-1 release from AIA acts directly or indirectly on AWC sensory neurons to limit their activity.

Discussion

Many neurons release both classical neurotransmitters and neuropeptides34–36. Our results suggest that AWC releases both the classical neurotransmitter glutamate and the neuropeptide NLP-1 to modulate behavior (Fig S4e). The glutamate signaling pathway promotes local search and odor chemotaxis, whereas the neuropeptide pathway limits local search and promotes odor adaptation. Glutamate signals are interpreted by multiple glutamate receptors on interneurons9, and NLP-1 is sensed by NPR-11 on AIA interneurons, which release INS-1 that directly or indirectly limits AWC activity and behavior. In one straightforward model, INS-1 is released from active AIA neuron when odor is present; the INS-1 released during a short odor exposure inhibits repetitive calcium transients from AWC when odor is removed, and the prolonged INS-1 release during a long odor exposure has a stronger effect, completely suppressing AWC calcium transients upon subsequent odor removal. This feedback loop may act as a gain control circuit to dampen AWC output to

strong stimuli, a role that negative feedback plays in other neuronal systems[37]. In this interpretation, the increased oscillations in *nlp-1* and other mutants result from ungoverned high-gain signaling in AWC.

A number of inhibitory pathways involving a single neuropeptide are known; this pathway is unusual in its apparent requirement for two neuropeptides from two neurons, working in a feedback loop. Several properties of this feedback loop remain to be determined. For example, we do not know when NLP-1 and INS-1 are released with respect to food or odor cues, and with respect to AWC and AIA activity. If the peptides are released when the neurons are active, NLP-1 would be released in alternation with INS-1 and not simultaneously; the slow biochemical timescale of G protein signaling may permit temporal integration across asynchronous activity of AWC and AIA[38]. Another missing component of the feedback model is the receptor for INS-1, as mutation of the one characterized *C. elegans* insulin receptor gene, *daf-2*, did not mimic or suppress *ins-1* mutations as predicted for an *ins-1* receptor (data not shown). *ins-1* antagonizes *daf-2* in the developmental dauer larva pathway[39], and can act either as an agonist or an antagonist of *daf-2* in food-regulated thermal learning and salt learning paradigms[33, 40], but *C. elegans* has over 30 insulin-regulated peptides, and *daf-2* may not be the only receptor for this peptide family. Precedent for alternative insulin receptors exists in mammals, where GPCRs are receptors for the insulin-related relaxin peptides[41].

The behavioral functions of *ins-1* in AWC olfactory adaptation are related to its previously described functions during ASE salt chemotaxis learning, where *ins-1* from AIA suppresses chemotaxis after salt is paired with starvation[33]. It will be interesting to ask whether NLP-1 or another sensory peptide initiates ASE salt chemotaxis learning, and whether *ins-1* signaling alters ASE sensory dynamics. Although we specifically examined the relationship between AWC and AIA, the AIA interneurons also receive synaptic input from neurons that sense food, tastants, pheromones, and repellents[1, 33, 42]. This connectivity might enable AIA to act as a local integrator of sensory information.

Increasing evidence in many animals indicates that peripheral olfactory signaling is modulated by top-down signals, internal states, and neuromodulators. State-dependent inputs affect olfactory signaling in rodents, acting as early as the synapses of the olfactory sensory neurons[43,44]. In *Drosophila*, tachykinin peptides expressed by local interneurons mediate presynaptic inhibition of olfactory receptor neurons[45]. The modulation of primary sensory neurons is a prominent feature of pain-sensing pathways[46]; we suggest that it will also be prominent in olfactory systems. In *C. elegans*, the use of specific mutants allows these feedback mechanisms to be directly linked to olfactory responses and behaviors, and also reveals their functional diversity. The neuropeptide feedback loop described here acts to dampen AWC output, while a different modulatory pathway involving the receptor guanylate cyclase GCY-28 can regulate an AWC switch from behavioral attraction to repulsion[8]. The *C. elegans* genome contains about 113 genes that encode more than 250 predicted neuropeptides, a rich potential source of behavioral variability[10, 47, 48].

The experiments described here reveal neuropeptide-regulated dynamic properties of *C. elegans* neurons that correlate with the dynamics of behavior. The prolonged AWC calcium

signals in *nlp-1, npr-11*, and *ins-1* mutants correlate with their increased turning during local search behavior. The reduced AWC calcium signals after prolonged odor exposure correlate with olfactory adaptation, which is reduced in *nlp-1, npr-11*, and *ins-1* mutants. Further studies of the AWC circuit should generate a better understanding of the relationship between behavior and the time-varying acute responses of AIA, sustained responses of AIB, and repetitive responses of AWC and AIY9. Together with previous results in *C. elegans* mechanosensory neurons49, these results suggest that circuit input tunes sensory responses to external stimuli based on sensory history and internal states, generating a rudimentary form of decision making.

Methods

Calcium imaging

To generate an AIA imaging line, GCaMP2.2b15 was expressed under the *gcy-28.d* promoter8, which is expressed strongly in AIA and weakly in RIA, ASK, AVJ, and other cells. The AWC GCaMP1 imaging line was described previously9. The lines were scored quantitatively for AWC local search behaviors, and those with normal responses were used for calcium imaging. Animals were trapped in a custom-designed microfluidic device made of the transparent polymer PDMS in which animals are restrained in a small chamber matching their dimensions, exposed to odors in liquid streams under laminar flow, and monitored using wide-field fluorescence microscopy9,22. Fluorescence from the cell of interest was captured after the presentation of isoamyl alcohol (10^{-4} dilution) and after odor removal five minutes later.

Metamorph and a Coolsnap HQ (Photometrics) camera were used to capture stacks of TIFF images at 10 frames/sec during the addition and removal of odor stimulus. A region of interest encompassing the cell was identified in all frames and the average fluorescence intensity recorded. A Matlab script used the data generated by MetaMorph to plot the imaging responses. The average fluorescence of the region of interest was generated by subtracting the recorded value from the average intensity of the background region of a similar area. The average fluorescence in a 3 second window (t=1–4s) was set as F_o. The percent change in the fluorescence intensity for the region of interest relative to F_o was plotted for all stacks, and these data were used for further analysis. Raw traces were corrected for fluorescence bleaching by subtracting a fixed correction function obtained by fitting an exponential curve to wild-type control traces using the equation: $y(t) = 100\%$ $(\exp(-t/\tau) - 1)$ where *t* is time and τ is time constant. Since bleaching rates were found to vary among neurons, separate time constants were obtained for AWC ($\tau = 330.7$ s; 95% confidence interval: $327.1 - 334.4$ s; $R^2 = 0.91$) and AIA ($\tau = 615.5$ s; 95% confidence interval: $607.2 - 623.8$ s; $R^2 = 0.86$).

Because the irregular secondary calcium transients in AWC were not visible in averaged traces, the ratio of change in fluorescence to total fluorescence for individual traces were plotted in heat maps in Fig. 3 and Supplementary Figs. S1 and S4. The wild-type controls for each figure were interleaved with mutants tested over the same time period.

Local search behavior

Individual animals were scored for exploratory behavior while in the presence of food (5 minutes), immediately after removal from food (1–12 minutes), and at long times off food (35–40 minutes)[6, 9]. All turns and reversals were scored by eye, by an investigator blind to the genotype of the animal. Reversals and turns were identified as described[6]. Results in Figs. 1 and 5 show turning rates scored 7–12 minutes after removal from food, and are reported as RevOmega values, which represent reversals coupled to omegas. Qualitatively similar results were obtained when large reversals or omega turns were scored individually (Supplementary Table 1). Data were analyzed using Perl scripts to calculate reversal and omega frequencies.

Adaptation assays

Adaptation assays were performed as previously described[26]. Animals were washed and plated on 3% assay agar plates. 16 µl of isoamyl alcohol was placed on agar plugs on the plate lid and the plates were sealed with parafilm (conditioning plate). After 60 min or 90 min, animals were washed and tested for chemotaxis on fresh plates. Controls were treated identically except that isoamyl alcohol was omitted from the conditioning plate. For imaging experiments, animals were conditioned for 60 min with or without isoamyl alcohol and then loaded into the device for calcium imaging.

Discrete Fourier transform

The plots in Figs. 3d,h, 5b, and Supplementary Figure S1 and S4d were generated by transforming data in the time domain (the raw fluorescence trace $y(t)$) into the frequency domain ($Y(f)$), using the Matlab function fft (discrete Fourier transform) which computes

$$Y(f_k) = \sum_{j=0}^{N-1} y(t_j) e^{\frac{-2\pi i}{N} kj} \text{ where } k = 0 \ldots N-1, N = 1200, \text{ and } i = \sqrt{-1}. \quad \text{(Eq. 1)}$$

at 1200 equally-spaced frequencies from $f_0 = 0$ to $f_{1199} = 10$ Hz, the sampling rate. Aliasing, or contribution from oscillatory components at higher than the Nyquist frequency (5Hz), is negligible based on the rapid drop-off of the Fourier transform with increasing frequency because the dynamics of calcium fluorescent indicators is slower than the sampling rate. The normalized energy spectral density, $|Y(f_k)|^2 / \sum_{f_1 \leq f_k \leq f_{N/2}} |Y(f_k)|^2,$ was then calculated for each trace and averaged across each group of traces at each f_k sample point to give

$\left\langle |Y(f_k)|^2 / \sum_{f_1 \leq f_k \leq f_{N/2}} |Y(f_k)|^2 \right\rangle_{\text{trials}}$ versus f_k (Figs. 3d, 3h and 5b). The value $|Y(f_0)|$ represents the mean of the entire time-domain vector $y(t)$ and was excluded from the calculation of energy spectral density normalization and band power ratio (described below), although including the value in the calculations did not significantly affect results. Values of f above $f_{N/2}$ were also excluded from calculations due to the redundancy of the magnitude of the second half of the discrete Fourier spectrum when performed on real-valued signals. For simplicity, no smoothing or windowing was applied to the energy spectral density. Applying various windowing schemes did not significantly affect quantifications (data not shown).

This representation of calcium signal data was chosen for two reasons: First, because calcium events were not registered in time, transients after the initial peak response were typically lost when averaging traces from multiple animals (Supplementary Figs. S2a, S2b). In contrast, the frequency-domain representation separates magnitude and phase information and secondary transients are preserved when averaging over many experiments. Second, this representation allows the identification and separation of signal components in various frequency bands. Low frequencies capture the magnitude of the primary response, high frequencies capture signal measurement noise, and middle frequencies capture secondary transients.

As an estimate of the portion of the total signal contributed by oscillatory components in a band bounded by two frequencies f_{min} and f_{max}, we compute the *band power ratio* as

$$Band\ Power\ Ratio(f_{min}, f_{max}) = \sum_{f_{min} \leq f_k \leq f_{max}} |Y(f_k)|^2 / \sum_{f_1 \leq f_k \leq f_{N/2}} |Y(f_k)|^2 \quad \text{(Eq. 2)}$$

The complete time domain trace $y(t)$ can be exactly reconstructed from its complex Fourier spectrum via the inverse discrete Fourier transform (Matlab function ifft) which computes:

$$y(t_j) = \frac{1}{N} \sum_{k=0}^{N-1} Y(f_k) e^{\frac{2\pi i}{N} kj} \text{ where } j = 0 \ldots N-1, N = 1200, \text{and } i = \sqrt{-1}. \quad \text{(Eq. 3)}$$

For visualizing signal contributions from each frequency band, Fourier spectra were divided into 3 frequency bands, and time-domain signals represented by the contributions from a single frequency band were reconstructed via the inverse discrete Fourier transform (Eq. 3) of the complex Fourier spectrum clipped to zero everywhere outside of the particular frequency band. Middle band reconstructions are shown in Supplementary Figures S1 and S4d. By mathematical identity, the sum of the low, middle, and high-frequency trace reconstructions equals the full time-domain fluorescence trace. Since reconstructions based on sharply clipped samples can potentially result in ringing effects (continued oscillations during a time period when the original trace is not oscillating), we also performed reconstructions using sloped frequency windows. No major changes in the appearance of trace reconstructions during the 30–120 sec period were observed (not shown).

The choice of middle frequency band range was made by separating the Fourier spectra into many bands (10 cutoffs at 0.001, 0.01, 0.02, 0.033, 0.1, 0.2, 0.5, 1, 2, 5 Hz) and selecting the bands that significantly distinguished wild type from *nlp-1* responses (data not shown). We found that most *nlp-1* secondary transients are captured in a narrower $f = 0.033 - 0.2$ Hz band, but *nlp-1* traces also show increased oscillation in the $f = 0.2 - 1$ Hz range; hence, the combination of these bands ($f = 0.033 - 1$ Hz) was selected as the region of interest for Supplementary Figs. S1 and S4d. This frequency range corresponds to periodic oscillations with periods between 1 and 30 s. The different genotypes do not show significant differences in the frequency domain less than 0.033Hz or greater than 1 Hz, suggesting little effect on the primary response or signal noise.

Three of the genotypes (*nlp-1*, *npr-11* and *ins-1*) showed strong secondary calcium transients. The *nlp-1* energy spectral density shows a broad peak in frequency-domain amplitude at $f = 0.0583$ Hz (Fig. 3d), corresponding to a period of 17s; this period is similar to the time period between large calcium transients determined by a manual measurement of *nlp-1* traces (19.5 ± 2.2 s (mean ± SD); Fig. 3b). Similarly, *npr-11* and *ins-1* animals show increased amplitude at frequencies corresponding to a period between 10 and 20 s (Fig 3f,h, Supplementary Figs. S4b,d). These transients were not observed during imaging of wild-type or *nlp-1* animals during buffer exchange protocols (Supplementary Fig. S1). All calculations were performed with Matlab (7.0R14, The MathWorks, Natick, MA).

Cell culture and calcium imaging

Two peptides, one corresponding to the NLP-1 sequence (MDANAFRMSFamide) and the second with a scrambled sequence (MSMRFANADFamide), were synthesized by the Proteomics resource center at The Rockefeller University. Human embryonic kidney 293 cells (HEK293) were cultured in DMEM supplemented with 10% FBS at 37°C in a humidified atmosphere containing 5% CO_2. 50–60% confluent cells were transfected with a 1:1 ratio of pME18s-*npr-11* and pcDNA3-α16Z (a promiscuous G-protein13, a kind gift from Prof. Y.H. Wang) using Lipofectamine 2000 and incubated for at least 24 hours; the transient transfection efficiency was ~70%, estimated by cotransfecting β2-adrenergic receptor and Gα15 plasmids and counting the fraction of cells responsive to isoproterenol. In control experiments, the receptor or G protein was transfected alone. Experiments were conducted on three plates for each condition on three different days. The transfected cells were loaded with 2.5uM fura-2/AM for 20 min at 37°C, peptide solution was applied sequentially to the cells for 15s with a peristaltic pump, and fluorescence at 510 nm by excitation at 340/380 nm was monitored by MetaFluor calcium imaging system. The calcium response trace was calculated using all cells in randomly chosen fields. For receptor and G protein transfections, ten fields were analyzed; for G protein alone, seven fields, and for receptor alone, eight fields.

Laser ablations

In transgenic animals expressing GCaMP2.2b under an AIA-specific promoter, AWC neurons were identified based on their position and morphology using Nomarski optics, and killed with a Micropoint laser system. Operated animals were tested in parallel with control animals from the same strain on the same day.

Molecular biology and transgenesis

cDNA or genomic regions corresponding to the entire coding sequences of *nlp-1*, *npr-11*, and *ins-1* were amplified by PCR from mRNA or genomic DNA and expressed under cell-specific promoters as indicated. For behavioral experiments in transgenic lines, a splice leader (SL2) fused to a gfp transgene was used to confirm cell-specific expression of the gene of interest, and only animals expressing GFP were scored. Selective expression in AWC, ASI, AIA or AIY was achieved using the promoters *odr-3* (AWC>AWB), *str-3* (ASI alone), *gcy-28.d* (AIA) and *ttx-3* (AIY alone). Germline transformations were carried out my

microinjection of plasmids at concentrations between 10 ng/μl and 50 ng/μl. Strains were grown and maintained under standard conditions50.

Supplementary Material

Refer to Web version on PubMed Central for supplementary material.

Acknowledgements

References

1. White JG, Southgate E, Thomson JN, Brenner S. The structure of the nervous system of the nematode *Caenorhabditis elegans*. Phil. Transact. R. Soc. Lond. B. 1986; 314:1–340.

2. Chalfie M, et al. The neural circuit for touch sensitivity in *Caenorhabditis elegans*. J Neurosci. 1985; 5:956–964. [PubMed: 3981252]

3. Bargmann, CI. Chemosensation in *C. elegans*. WormBook; 2006. p. 1-29.ed. The C. elegans research community, doi/10.1895/wormbook.1.123.1, http://www.wormbook.org

4. Bargmann CI, Hartwieg E, Horvitz HR. Odorant-selective genes and neurons mediate olfaction in *C. elegans*. Cell. 1993; 74:515–527. [PubMed: 8348618]

5. Wakabayashi T, Kitagawa I, Shingai R. Neurons regulating the duration of forward locomotion in *Caenorhabditis elegans*. Neurosci Res. 2004; 50:103–111. [PubMed: 15288503]

6. Gray JM, Hill JJ, Bargmann CI. A circuit for navigation in *Caenorhabditis elegans*. Proc Natl Acad Sci U S A. 2005; 102:3184–3191. [PubMed: 15689400]

7. Pierce-Shimomura JT, Morse TM, Lockery SR. The fundamental role of pirouettes in *Caenorhabditis elegans* chemotaxis. J Neurosci. 1999; 19:9557–9569. [PubMed: 10531458]

8. Tsunozaki M, Chalasani SH, Bargmann CI. A behavioral switch: cGMP and PKC signaling in olfactory neurons reverses odor preference in *C. elegans*. Neuron. 2008; 59:959–971. [PubMed: 18817734]

9. Chalasani SH, et al. Dissecting a circuit for olfactory behaviour in *Caenorhabditis elegans*. Nature. 2007; 450:63–70. [PubMed: 17972877]

10. Nathoo AN, Moeller RA, Westlund BA, Hart AC. Identification of neuropeptide-like protein gene families in *Caenorhabditis elegans* and other species. Proc Natl Acad Sci U S A. 2001; 98:14000–14005. [PubMed: 11717458]

11. Wenick AS, Hobert O. Genomic cis-regulatory architecture and trans-acting regulators of a single interneuron-specific gene battery in *C. elegans*. Dev Cell. 2004; 6:757–770. [PubMed: 15177025]

12. Etchberger JF, et al. The molecular signature and cis-regulatory architecture of a *C. elegans* gustatory neuron. Genes Dev. 2007; 21:1653–1674. [PubMed: 17606643]

13. Mody SM, Ho MK, Joshi SA, Wong YH. Incorporation of Galpha(z)-specific sequence at the carboxyl terminus increases the promiscuity of galpha(16) toward G(i)-coupled receptors. Mol Pharmacol. 2000; 57:13–23. [PubMed: 10617674]

14. Tallini YN, et al. Imaging cellular signals in the heart in vivo: Cardiac expression of the high-signal Ca2+ indicator GCaMP2. Proc Natl Acad Sci U S A. 2006; 103:4753–4758. [PubMed: 16537386]

15. Tian L, et al. Imaging neural activity in worms, flies and mice with improved GCaMP calcium indicators. Nature Methods. 2009:875–881. [PubMed: 19898485]

16. Lockery SR, Goodman MB. The quest for action potentials in *C. elegans* neurons hits a plateau. Nat Neurosci. 2009; 12:377–378. [PubMed: 19322241]

17. Suzuki H, et al. In vivo imaging of *C. elegans* mechanosensory neurons demonstrates a specific role for the MEC-4 channel in the process of gentle touch sensation. Neuron. 2003; 39:1005–1017. [PubMed: 12971899]

18. O'Hagan R, Chalfie M, Goodman MB. The MEC-4 DEG/ENaC channel of *Caenorhabditis elegans* touch receptor neurons transduces mechanical signals. Nat Neurosci. 2005; 8:43–50. [PubMed: 15580270]

19. Clark DA, Biron D, Sengupta P, Samuel AD. The AFD sensory neurons encode multiple functions underlying thermotactic behavior in *Caenorhabditis elegans*. J Neurosci. 2006; 26:7444–7451. [PubMed: 16837592]

20. Ramot D, MacInnis BL, Goodman MB. Bidirectional temperature-sensing by a single thermosensory neuron in *C. elegans*. Nat Neurosci. 2008; 11:908–915. [PubMed: 18660808]

21. Mellem JE, Brockie PJ, Zheng Y, Madsen DM, Maricq AV. Decoding of polymodal sensory stimuli by postsynaptic glutamate receptors in *C. elegans*. Neuron. 2002; 36:933–944. [PubMed: 12467596]

22. Chronis N, Zimmer M, Bargmann CI. Microfluidics for in vivo imaging of neuronal and behavioral activity in *Caenorhabditis elegans*. Nat Methods. 2007; 4:727–731. [PubMed: 17704783]

23. Horoszok L, Raymond V, Sattelle DB, Wolstenholme AJ. GLC-3: a novel fipronil and BIDN-sensitive, but picrotoxinin-insensitive, L-glutamate-gated chloride channel subunit from *Caenorhabditis elegans*. Br J Pharmacol. 2001; 132:1247–1254. [PubMed: 11250875]

24. Lee RY, Sawin ER, Chalfie M, Horvitz HR, Avery L. EAT-4, a homolog of a mammalian sodium-dependent inorganic phosphate cotransporter, is necessary for glutamatergic neurotransmission in *Caenorhabditis elegans*. J Neurosci. 1999; 19:159–167. [PubMed: 9870947]

25. Sieburth D, Madison JM, Kaplan JM. PKC-1 regulates secretion of neuropeptides. Nat Neurosci. 2007; 10:49–57. [PubMed: 17128266]

26. Colbert HA, Bargmann CI. Odorant-specific adaptation pathways generate olfactory plasticity in *C. elegans*. Neuron. 1995; 14:803–812. [PubMed: 7718242]

27. Colbert HA, Smith TL, Bargmann CI. OSM-9, a novel protein with structural similarity to channels, is required for olfaction, mechanosensation, and olfactory adaptation in *Caenorhabditis elegans*. J Neurosci. 1997; 17:8259–8269. [PubMed: 9334401]

28. L'Etoile ND, et al. The cyclic GMP-dependent protein kinase EGL-4 regulates olfactory adaptation in *C. elegans*. Neuron. 2002; 36:1079–1089. [PubMed: 12495623]

29. Palmitessa A, et al. *Caenorhabditis elegans* arrestin regulates neural G protein signaling and olfactory adaptation and recovery. J Biol Chem. 2005; 280:24649–24662. [PubMed: 15878875]

30. Matsuki M, Kunitomo H, Iino Y. Goalpha regulates olfactory adaptation by antagonizing Gqalpha-DAG signaling in *Caenorhabditis elegans*. Proc Natl Acad Sci U S A. 2006; 103:1112–1117. [PubMed: 16418272]

31. Yamada K, Hirotsu T, Matsuki M, Kunitomo H, Iino Y. GPC-1, a G protein gamma-subunit, regulates olfactory adaptation in *Caenorhabditis elegans*. Genetics. 2009; 181:1347–1357. [PubMed: 19189947]

32. Kaye JA, Rose NC, Goldsworthy B, Goga A, L'Etoile ND. A 3'UTR pumilio-binding element directs translational activation in olfactory sensory neurons. Neuron. 2009; 61:57–70. [PubMed: 19146813]

33. Tomioka M, et al. The insulin/PI 3-kinase pathway regulates salt chemotaxis learning in *Caenorhabditis elegans*. Neuron. 2006; 51:613–625. [PubMed: 16950159]

34. Marder E, Bucher D. Understanding circuit dynamics using the stomatogastric nervous system of lobsters and crabs. Annu Rev Physiol. 2007; 69:291–316. [PubMed: 17009928]

35. Nassel DR, Homberg U. Neuropeptides in interneurons of the insect brain. Cell Tissue Res. 2006; 326:1–24. [PubMed: 16761145]

36. Burnstock G. Cotransmission. Curr Opin Pharmacol. 2004; 4:47–52. [PubMed: 15018838]

37. Demb JB. Functional circuitry of visual adaptation in the retina. J Physiol. 2008; 586:4377–4384. [PubMed: 18617564]

38. Stein W, DeLong ND, Wood DE, Nusbaum MP. Divergent co-transmitter actions underlie motor pattern activation by a modulatory projection neuron. Eur J Neurosci. 2007; 26:1148–1165. [PubMed: 17767494]

39. Pierce SB, et al. Regulation of DAF-2 receptor signaling by human insulin and ins-1, a member of the unusually large and diverse *C. elegans* insulin gene family. Genes Dev. 2001; 15:672–686. [PubMed: 11274053]

40. Kodama E, et al. Insulin-like signaling and the neural circuit for integrative behavior in *C. elegans*. Genes Dev. 2006; 20:2955–2960. [PubMed: 17079685]

41. Ivell R, Einspanier A. Relaxin peptides are new global players. Trends Endocrinol Metab. 2002; 13:343–348. [PubMed: 12217491]

42. Macosko EZ, et al. A hub-and-spoke circuit drives pheromone attraction and social behaviour in *C. elegans*. Nature. 2009; 458:1171–1175. [PubMed: 19349961]

43. Wachowiak M, Wesson DW, Pirez N, Verhagen JV, Carey RM. Low-level mechanisms for processing odor information in the behaving animal. Ann NY Acad Sci. 2009; 1170:286–292. [PubMed: 19686149]

44. Gomez C, et al. Heterogeneous targeting of centrifugal inputs to the glomerular layer of the main olfactory bulb. J Chem Neuroanat. 2005; 29:238–254. [PubMed: 15927786]

45. Ignell R, et al. Presynaptic peptidergic modulation of olfactory receptor neurons in *Drosophila*. Proc Natl Acad Sci U S A. 2009; 106:13070–13075. [PubMed: 19625621]

46. Stein C, et al. Peripheral mechanisms of pain and analgesia. Brain Res Rev. 2009; 60:90–113. [PubMed: 19150465]

47. Li, C.; Kim, K. Neuropeptides. WormBook; 2008. p. 1-36.ed. The C. elegans research community, doi/10.1895/wormbook.1.142.1, http://www.wormbook.org

48. Li C, Nelson LS, Kim K, Nathoo A, Hart AC. Neuropeptide gene families in the nematode *Caenorhabditis elegans*. Ann N Y Acad Sci. 1999; 897:239–252. [PubMed: 10676452]

49. Kindt KS, et al. Dopamine mediates context-dependent modulation of sensory plasticity in *C. elegans*. Neuron. 2007; 55:662–676. [PubMed: 17698017]

50. Brenner S. The genetics of *Caenorhabditis elegans*. Genetics. 1974; 77:71–94. [PubMed: 4366476]
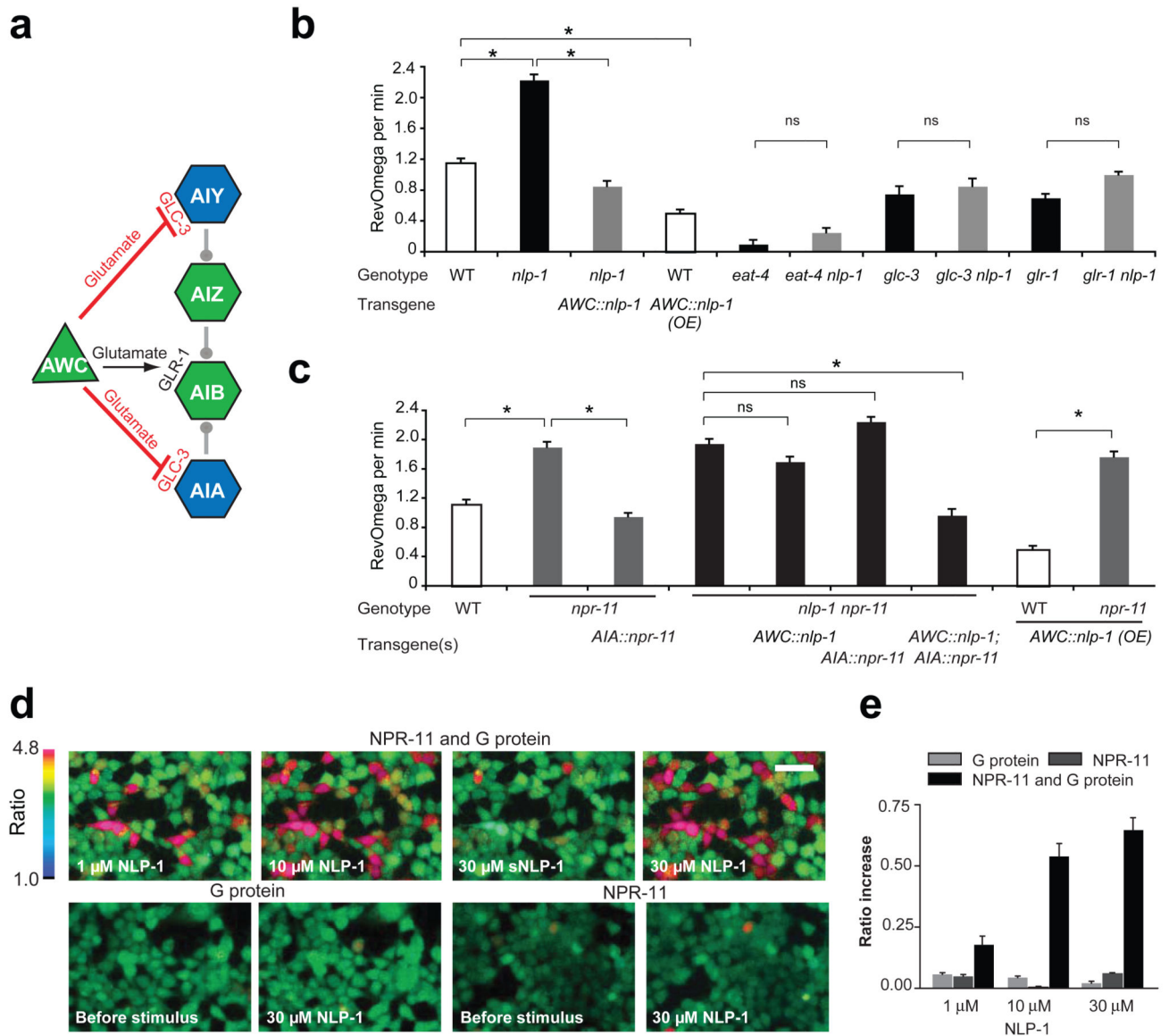
Figure 1. AWC releases NLP-1, which acts on NPR-11 in AIA

(a) AWC sensory neurons, downstream interneurons, and relevant glutamate receptors (from this work (AIA) and from ref9). (b,c) Local search behavior 7–12 minutes after removal from food. RevOmega, coupled reversal-omega behaviors characteristic of local search. Analysis of *nlp-1* mutants (b) and *npr-11* mutants (c). In all figures, WT indicates control N2 strain, *AWC::nlp-1* indicates *nlp-1* cDNA under AWC-selective *odr-3* promoter, *AWC::nlp-1(OE)* indicates the same plasmid injected at high concentrations, *AIA::npr-11* indicates *npr-11* cDNA under AIA-selective *gcy-28.d* promoter. Error bars indicate s.e.m.; asterisks mark comparisons different at P< 0.05 by t-test or t-test with Bonferroni correction, as appropriate. Complete behavioral data with all genotypes and timepoints are in Supplementary Table 1. (d,e) Response of *npr-11-* and Gα16Z-, *npr-11* or Gα16Z-transfected HEK 293 cells to an NLP-1 peptide and a scrambled NLP-1 peptide (sNLP-1).

(d) Pseudo-color images of fura2-labeled cells indicating fluorescent ratio intensities. Scale bar, 100 μm. (e) Average calcium response of all cells in the window (n=10 fields for *npr-11* and Gα16Z, n=8 for *npr-11* and n=7 for Gα16Z). Averages and s.e.m. are shown.
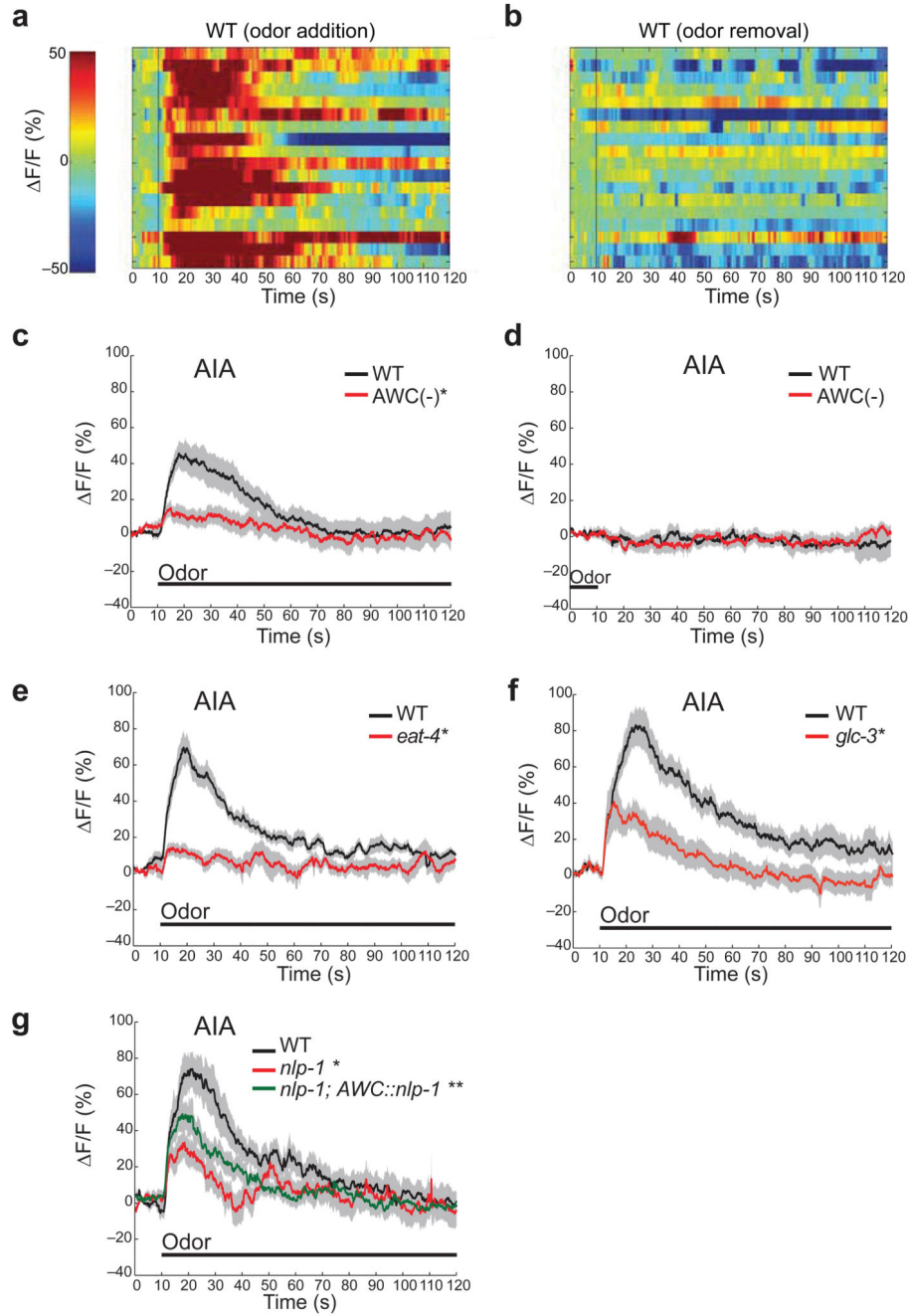
Figure 2. Calcium responses in AIA interneurons require AWC glutamate and NLP-1
(a,b) Heat maps showing the ratio of change in fluorescence to total fluorescence in AIA neurons expressing GCaMP2.2b15; (a) addition and (b) removal of odor stimulus at t =10s in each recording (n=18). (c,d) Average GCaMP fluorescence change in AIA neurons in wild-type (n=18) and wild-type AWC-ablated animals (n=12) on addition (c) and removal (d) of odor. (e–g) Mutant AIA responses. (e) *eat-4* (n=18, wt control n=18) (f) *glc-3* (n=16, wt control n=16) (g) *nlp-1* (n=18, wt control n=18) and *AWC::nlp-1* cell-selective rescue (n=18). In all imaging figures, "odor" is a 10^{-4} dilution of isoamyl alcohol. Light grey

shading indicates s.e.m. One asterisk marks results significantly different from wild type, and two asterisks mark results significantly different from *nlp-1* mutant ($P < 0.05$, t-test with Bonferroni correction).
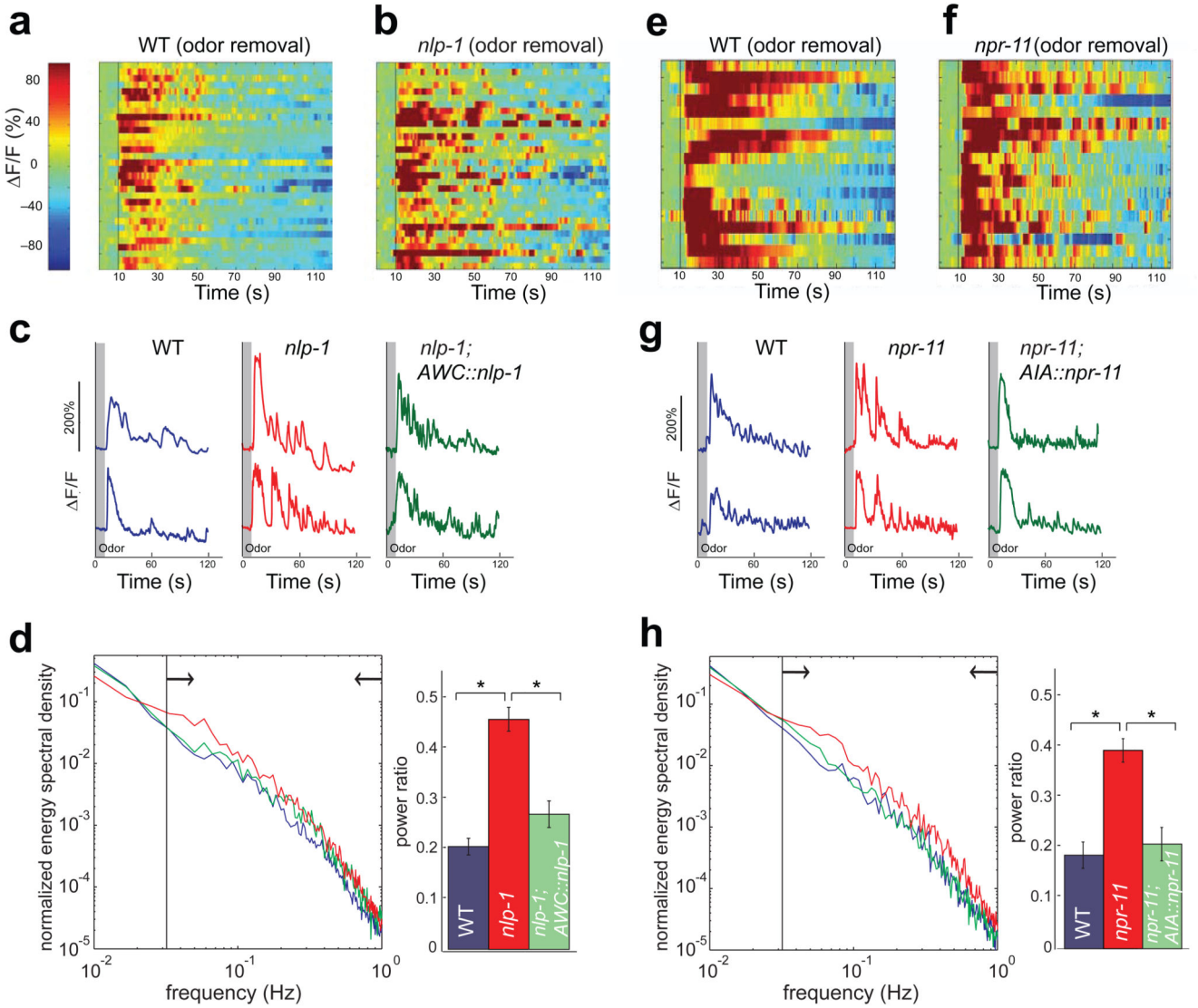
Figure 3. Altered AWC calcium responses in *nlp-1* and *npr-11* mutants
(a,b,e,f) Heat maps showing ratio change in fluorescence to total fluorescence in AWC neurons expressing GCaMP1.0. Odor was removed at 10s in each recording. (a) Wild type (n=32) (b) *nlp-1* (n=32) (e) wild type (n=18) and (f) *npr-11* (n=18). (c,g) Representative AWC calcium responses from individual wild-type animals, (c) *nlp-1* and (g) *npr-11* mutants, and rescued strains. (d,h) Fourier power analysis of AWC calcium responses in (d) *nlp-1* and (h) *npr-11* mutants. Left, the normalized energy density spectrum averaged across all calcium traces of each genotype; arrows indicate range of the middle frequency band (color code is at right). Right, the average power ratio of the middle frequency band (0.033 Hz-1 Hz) across all calcium traces of each genotype; error bars indicate s.e.m. Asterisk marks comparisons different at *P*< 0.05 (t-test with Bonferroni correction).
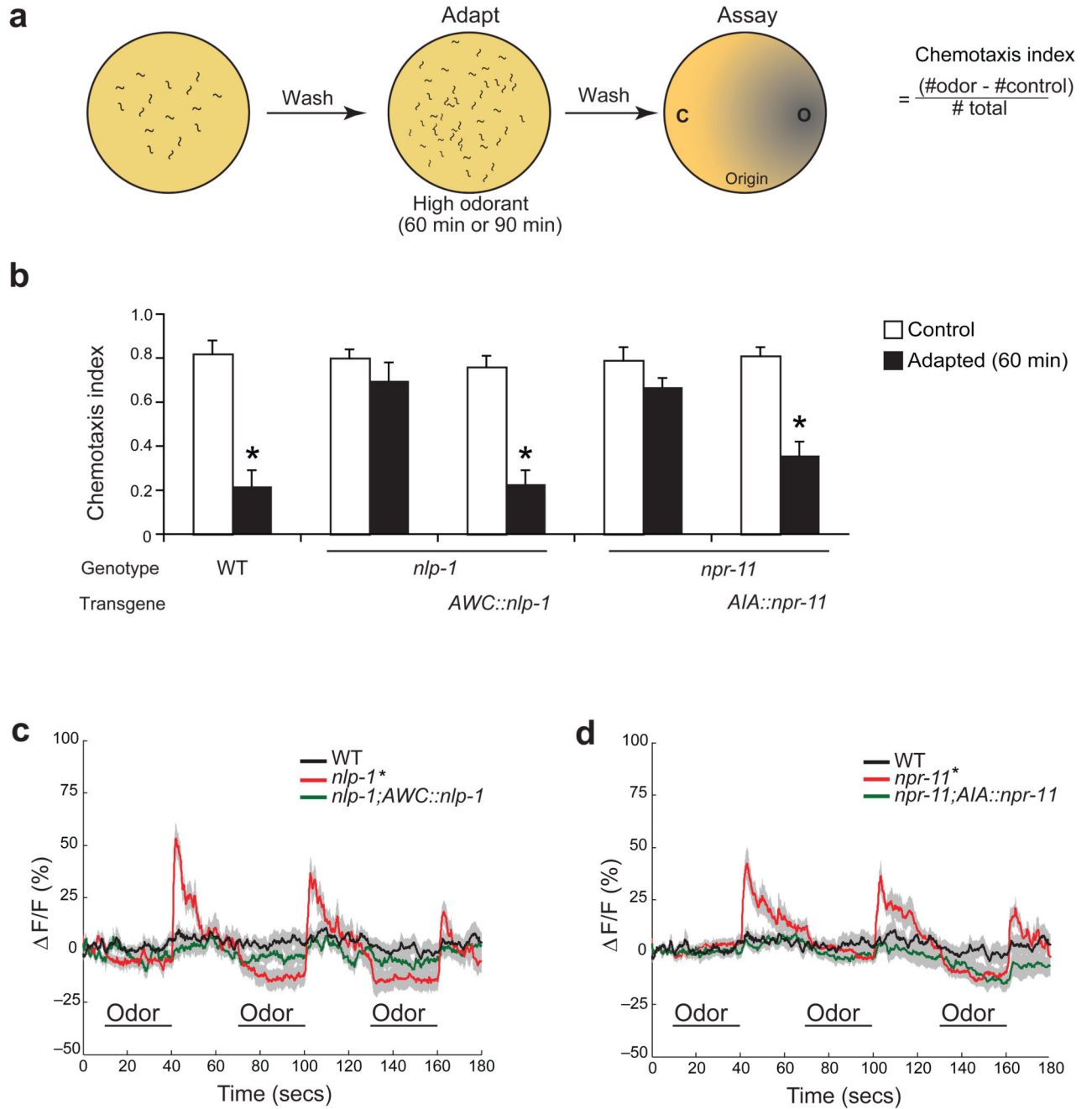
Figure 4. *nlp-1* and *npr-11* are defective in olfactory adaptation
(a) Schematic diagram of adaptation assay. (b) Adaptation in *nlp-1* and *npr-11* mutants, and cell-selective rescue. Error bars indicate s.e.m. Asterisk marks results significantly comparisons different at *P*< 0.05 (t-test with Bonferroni correction). (c, d) AWC calcium responses in wild-type, *nlp-1* and *AWC::nlp-1* transgenic rescued animals (c) and wild-type, *npr-11* and *AIA::npr-11* transgenic rescued animals (d) adapted for 60 min (n=12 each). Odor pulses are marked. Light grey shading indicates s.e.m. Asterisk marks results significantly different from wild-type (P<0.05, t-test with Bonferroni correction).
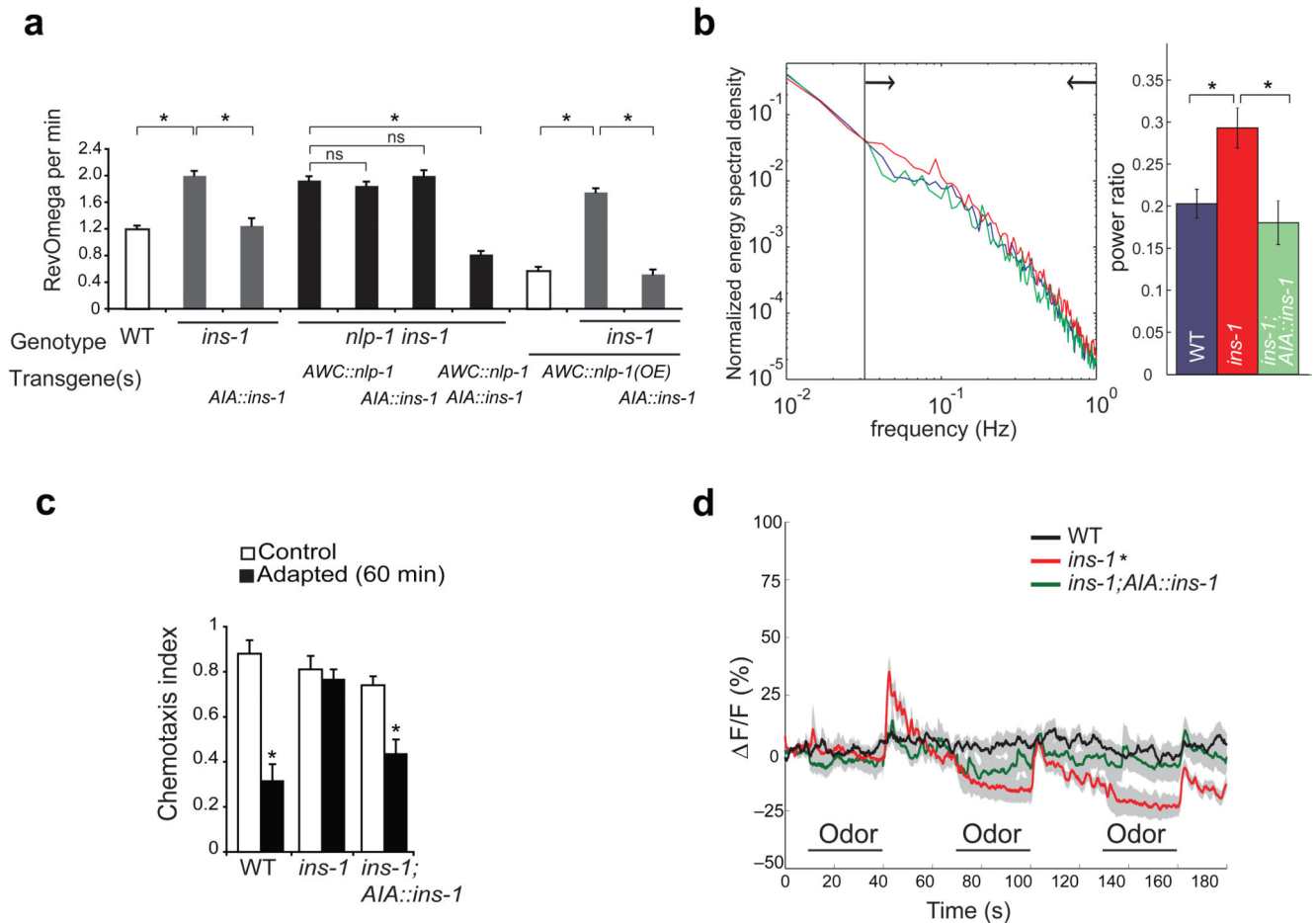
Figure 5. *ins-1* is a component of the *nlp-1-npr-11* pathway
(a) Local search behavior 7–12 minutes after removal from food. RevOmega, coupled reversal-omega behaviors characteristic of local search. *AIA::ins-1*, *ins-1* cDNA expressed under AIA-selective *gcy-28.d* promoter. Error bars indicate s.e.m. Asterisks mark relevant comparisons (P<0.05, t-test with Bonferroni correction.) (b) Fourier power analysis of AWC calcium responses in *ins-1* mutants. Left, the normalized energy density spectrum averaged across all calcium traces of each genotype; arrows indicate range of the middle frequency band (color code is at right). Right, the average power ratio of the middle frequency band (0.033 Hz-1 Hz) across all calcium traces of each genotype; error bars indicate s.e.m. Asterisk marks comparisons different at *P*< 0.05 (t-test with Bonferroni correction). (c) Adaptation in *ins-1* mutants, and cell-selective rescue. Asterisks mark results different from un-adapted control (P<0.05, t-test). Error bars indicate s.e.m. (d) AWC calcium responses in wild-type, *ins-1* and *AIA::ins-1* rescued transgenic animals adapted for 60 min (n=12 each). Odor pulses are marked. Light grey shading indicates s.e.m. Asterisk marks result different from wild type at P<0.05, t-test with Bonferroni correction.